electronics

MDPI

Article

# Research on Fast Frequency Response Control Strategy of Hydrogen Production Systems

**Tao Shi [1,2,*], Zeyan Xu [1], Libo Gu [1] and Hangyu Zhou [1]**

1 College of Automation, Nanjing University of Posts and Telecommunications, Nanjing 210023, China; 1222056624@njupt.edu.cn (Z.X.); 1222056621@njupt.edu.cn (L.G.); 1022051527@njupt.edu.cn (H.Z.)
2 Institute of Advance Technology for Carbon Neutrality, Nanjing University of Posts and Telecommunications, Nanjing 210023, China
* Correspondence: shitao@njupt.edu.cn

**Abstract:** With the large-scale integration of intermittent renewable energy generation presented by wind and photovoltaic power, the security and stability of power system operations have been challenged. Therefore, this article proposes a control strategy of a hydrogen production system based on renewable energy power generation to enable the fast frequency response of a grid. Firstly, based on the idea of virtual synchronous control, a fast frequency response control transformation strategy for the grid-connected interface of hydrogen production systems for renewable energy power generation is proposed to provide active power support when the grid frequency is disturbed. Secondly, based on the influence of VSG's inertia and damping coefficient on the dynamic characteristics of the system, a VSG adaptive control model based on particle swarm optimization is designed. Finally, based on the Matlab/Simulink platform, a grid-connected simulation model of hydrogen production systems for renewable energy power generation is established. The results show that the interface-transformed electrolytic hydrogen production device can actively respond to the frequency disturbances of the power system and participate in primary frequency control, providing active support for the frequency stability of the power system under high-percentage renewable energy generation integration. Moreover, the system with parameter optimization has better fast frequency response control characteristics.

**Keywords:** hydrogen production system; fast frequency response; virtual synchronous control; VSG adaptive control; particle swarm optimization



**Citation:** Shi, T.; Xu, Z.; Gu, L.; Zhou, H. Research on Fast Frequency Response Control Strategy of Hydrogen Production Systems. *Electronics* **2024**, *13*, 956. https://doi.org/10.3390/electronics13050956

Academic Editors: Temitayo Olowu and Raghav Khanna

Received: 6 February 2024
Revised: 26 February 2024
Accepted: 28 February 2024
Published: 1 March 2024



## 1. Introduction

With the large-scale grid connection of intermittent renewable energy generation presented by wind power and photovoltaics, system operation risks have emerged, along with the frequent absence of wind and sunlight [1,2]. On the one hand, the intermittent, random, and volatile nature of renewable energy power generation increases the flexible regulation demand of the power system. The system needs to configure additional regulatory resources to increase the absorption capacity of renewable energy. On the other hand, renewable energy power generation serves as a power electronic interface for power supply, which does not possess the inertia, damping, and primary frequency control support capabilities of traditional synchronous generators under conditions of disturbance.

Hydrogen energy, as a widely available, clean, carbon-free, flexible, and application-rich secondary energy source, is an essential carrier for supporting energy transformation and in building a modern energy system. We can realize the full utilization of renewable energy and alleviate the phenomenon of abandoned wind and abandoned light by closely integrating the hydrogen production strategy through electrolysis with the fluctuation of renewable energy output. Secondly, electrolytic hydrogen production serves as a flexible load regulation and storage solution, providing high-quality resources with flexible adjustments for new power systems. The hydrogen production device can serve as an energy storage carrier for renewable energy conversion. Combining electrolytic water with renewable energy generation can store excess electrical energy as chemical energy in hydrogen, thereby stabilizing renewable energy power fluctuations, increasing absorption capacity, and promoting clean energy.

There has been preliminary progress in the research of hydrogen generation from renewable energy power generation, both domestically and internationally. In ref. [3], to address the issues of wind turbine and photovoltaic power fluctuation, a grid-connected structure with an electrolyzer and supercapacitor assembled on a DC bus is constructed. A coordinated control model for the hybrid system is established, and the accuracy and effectiveness of the wind/PV/hydrogen production/supercapacitor grid-connected system model and control strategies are verified through Simulink simulations. In ref. [4], a refined model of electrolyzer participation in grid frequency control isestablished, and the fast frequency response capability of the electrolyzer is studied. In ref. [5], combining wind turbines with batteries and alkaline electrolyzer, a comprehensive control scheme for effectively managing the operation of the hydrogen generation system is proposed. In ref. [6], a virtual inertia and droop characteristic mechanism of the wind-storing hydrogen station is proposed to simulate a synchronous unit, followed by the establishment of a mathematical model for an alkaline electrolyzer, analyzing the matching between different energy storage devices and their synergistic effects in grid frequency control. In ref. [7], the authors compare the regulatory characteristics of alkaline electrolyzers and proton-exchange membrane (PEM) electrolyzers, and propose a dynamic power-allocation-control strategy for a hybrid system of both types of electrolyzers. In ref. [8], a comparative evaluation of fast active power-regulation-control strategies implemented on megawatt-scale controllable electrolyzers is presented, with the goal of achieving enhanced frequency support during large active power imbalances that lead to main low-frequency deviations. In ref. [9], the authors studied the coupling structure of wind turbines and electrolyzers, and compared the response characteristics of four different electrolyzer models under variable wind speed and grid fluctuation conditions. In ref. [10], a control strategy for a photovoltaic energy-storing grid-connected system based on a virtual synchronous generator has been proposed, which effectively suppresses the output power fluctuations of the photovoltaic inverter by coordinating the control of the energy storage unit. The above examples of the literature have demonstrated that controlling the electrolytic hydrogen system can stabilize the grid-connected power fluctuations of renewable energy sources. However, most of these studies consider using dispatch instructions to make the electrolytic hydrogen production device operate passively, without fully utilizing the inherent characteristics of the system. There is therefore a lack of active regulation capability for grid frequency.

In order to enable a renewable energy power-generation hydrogen production system to have a primary frequency-control active-response characteristic, the VSG control strategy is combined with the renewable energy power-generation hydrogen production system. The VSG control technology simulates the rotor motion characteristics of traditional synchronous generators and introduces a virtual inertia coefficient and damping coefficient into the control system through algorithms, thereby improving the system's frequency and voltage-regulation capabilities [11]. Compared with traditional synchronous generators, virtual synchronous generators are more flexible because they can change control parameters. During operation, changing control parameters to achieve a more stable performance and response speed greatly increases the flexibility of VSGs. The adaptive control method of rotor inertia and damping coefficient is based on this idea [12]. In ref. [13], a control strategy based on adaptive rotational inertia for VSGs has been proposed, which, compared with the traditional VSG method, has better stability, a faster response speed, and a smaller overshoot. In ref. [14], a VSG-coordination adaptive control strategy for rotational inertia and damping coefficient has been proposed, which effectively improves the dynamic regulation performance of the entire system. However, the above articles do not consider the impact of initial rotational inertia and damping coefficient on the system.

This paper uses the particle swarm optimization to optimize the initial damping coefficient and rotational inertia of the VSG, thus improving the dynamic response characteristics of the VSG. When combining the renewable energy power-generation hydrogen production system with it, the entire system can not only alleviate the phenomenon of abandoned wind and sunlight, but also actively provide frequency support for the grid.

## 2. Model of Electrolytic Hydrogen Production Systems

### *2.1. Principle of Electrolytic Hydrogen Production*

Electrolytic hydrogen production is a mature technology for hydrogen production within the industry. It involves the supply of electrical energy to enable the electrochemical reaction of water molecules in the electrolytic cell, resulting in the decomposition of hydrogen and oxygen. The water decomposition reaction primarily consists of two half-reactions: hydrogen evolution at the cathode and oxygen precipitation at the anode. The reaction equations are presented as follows [15]:

Anode: $2H_2O - \rightarrow 4H^+ + O_2 + 4e$.

Cathode: $4H^+ + 4e \rightarrow 2H_2$.

Total: $2H_2O - \rightarrow 2H_2 + O_2$.

Hydrogen production systems that utilize renewable energy for power generation not only makes the electrolytic hydrogen production process more energy-efficient and environmentally friendly, achieving "zero carbon emissions", but also transform intermittent and unstable renewable energy into stable and easily stored chemical energy. This approach solves the imbalance between long-term power supply and consumption, alleviates the limitation of grid output capacity on renewable energy power-generation systems, and realizes more effective development and utilization of renewable energy.

### *2.2. Simulation Model*

#### 2.2.1. Model of PEM Electrolyzer

The electrolyzer is a device that uses electrical energy to split water into hydrogen and oxygen through electrochemical reactions. The structural principle is illustrated in Figure 1. The electrolyzer comprises multiple independent electrolyzer cells connected in series or parallel. This article initially calculates the working voltage required for each electrolyzer cell, as well as the hydrogen and oxygen production rates generated by the electrolyzer [16].

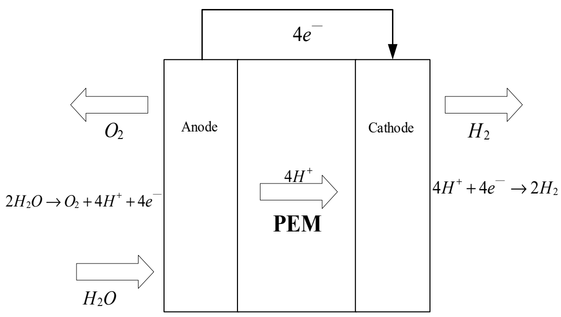


**Figure 1.** Electrolyzer basic structure.

Studying the I–V characteristics of an electrolyzer can significantly enhance the efficiency of gas production. From an electrical circuit perspective, an electrolyzer is equivalent to a voltage-sensitive, nonlinear DC load. After connecting to a power supply, the electrolyzer is linked to the DC bus via a DC/DC converter. The current and voltage characteristics of the electrolytic device are determined by the working temperature of the electrolyzer. Given the high nonlinearity of the current and voltage characteristics, curve fitting methods are commonly employed to simulate them. Considering its applicability in the field of electrical engineering, the voltage equation of a single electrolyzer is as follows [17]:

$$V_{cell} = E + V_{el,act} + V_{el,ohm} \tag{1}$$

where $E$ is open circuit voltage, $V_{el,act}$ is activation polarization voltage, and $V_{el,ohm}$ is ohmic polarization voltage.

Open circuit voltage is defined as the Nernst Equation:

$$E = E_0 + \frac{RT_{el}}{2F}\left[\ln\left(\frac{P_{H_2}P_{0.5\cdot O_2}}{\alpha H_2O}\right)\right] \tag{2}$$

$$E_0 = 1.229 - 0.009(T - 298.15) \tag{3}$$

where $E_0$ is the standard cell potential, $R$ is the universal gas constant, $T_{el}$ is the cell temperature, $\alpha_{H_2O}$ is the water activity between anode and electrolyzer (for simplicity, it is assumed here to be 1), $P_{H_2}$ is the cathode hydrogen pressure, $P_{0.5\cdot O_2}$ is the anode oxygen pressure, and $F$ is the Faraday constant.

The activation polarization voltage is obtained as follows:

$$V_{el,act} = \frac{RT_{el}}{2\alpha F}\ln\left(\frac{i}{i_0}\right) \tag{4}$$

where $\alpha$ is the charge transfer coefficient, $i$ is the current density, and $i_0$ is the exchange current density.

The ohmic polarization voltage is calculated as follows:

$$V_{el,ohm} = iR_{el,ohm} \tag{5}$$

where $R_{el,ohm}$ is the membrane resistance.

When combining multiple electrolysis cells in series and parallel to form an electrolysis tank stack, the total power consumption and terminal voltage of the entire system are calculated as follows:

$$\begin{cases} P_{el} = N_b \cdot V_{el} \cdot I_{cell} \\ V_{el} = N_c \cdot V_{cell} \end{cases} \tag{6}$$

where $I_{cell}$ is the electrolytic current; $N_b$ and $N_c$ are the parallel and series numbers of the electrolytic unit, respectively.

The current and voltage characteristics of an electrolyzer are dependent on its operating temperature. According to Faraday's law, the generation rate of hydrogen in the electrolyzer is directly proportional to the rate of electron transfer at the electrode.

$$n_{H_2} = \frac{n_F \cdot I_{cell} \cdot N_c \cdot N_b}{2F} \tag{7}$$

where $n_{H_2}$ is the output hydrogen flow; $n_F$ is the Faraday efficiency.

The ratio between the actual and theoretical maximum hydrogen gas amounts in an electrolyzer is called the Faraday efficiency. At a working temperature of 80 °C for the electrolyzer, the Faraday efficiency is as follows:

$$n_F = 96.5 \cdot \exp(0.09/I_{cell} - 75.5/I_{cell}^2) \tag{8}$$

### 2.2.2. Model of Hydrogen Storage Tank

When temperature changes during hydrogen charging and discharging are not considered, the storage capacity can be expressed as follows:

$$n_{sto}(t_1) = n_{sto}(t_0) + \int_{t_0}^{t_1} v_{sto}(t)dt \tag{9}$$

where $n_{sto}(t_0)$ and $n_{sto}(t_1)$ are the hydrogen storage capacities of the hydrogen storage tank at moments $t_0$ and $t_1$, respectively; $v_{sto}(t)$ is the net intake rate of the hydrogen storage tank at time $t$.

The hydrogen storage tank pressure is as follows:

$$P_{sto} = \frac{RT_{sto}}{V_{sto}} n_{sto} \tag{10}$$

where $P_{sto}$ is the hydrogen storage tank pressure, $R$ is the gas constant, $T_{sto}$ is the gas thermodynamic, and $V_{sto}$ is the hydrogen storage tank capacity.

#### 2.2.3. Electrolyzer Dynamic Characteristics

Figures 2 and 3 illustrate the dynamic response characteristics of the electrolyzer, demonstrating that hydrogen production varies with the changes in input current.

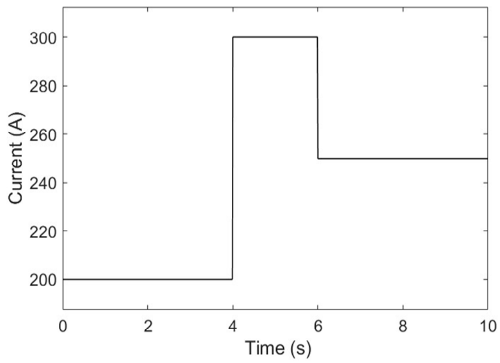


**Figure 2.** Input current of electrolyzer.

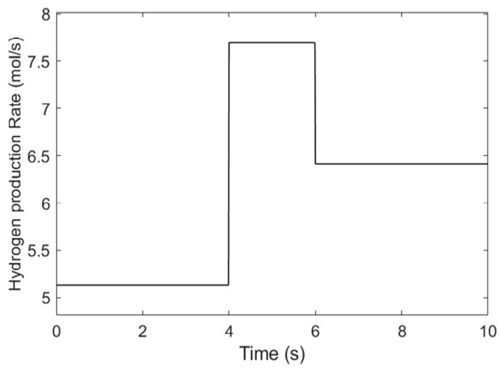


**Figure 3.** Hydrogen production rate of electrolyzer.

## 3. Objective of Fast Frequency Response Control

### *3.1. The Principle of Frequency Response*

The principle of primary frequency control in power systems is illustrated in Figure 4. When the balance of active power within the grid becomes disturbed, leading to a deviation in the grid's frequency from its rated value, the regulation systems of the parallel operating generating units or other frequency adjustment devices rapidly adjust their active power output according to their individual speed-regulated static and dynamic characteristics to swiftly restore the grid's active power balance.

As illustrated in Figure 4, $P_G(f)$ and $P_D(f)$ represent the frequency characteristics of the generator set and the total load, respectively. The system initially operates at point A, where at $P_G = P_D$, a power balance is maintained, and the frequency stays stable at the rated frequency $f_1$. When the system load increases by $\Delta P_{D0}$, the load's frequency characteristic shifts to $P'_D(f)$, resulting in a disruption of power balance. If left uncontrolled, the grid frequency will continue to decline. To mitigate the frequency drop, the generator set increases its output of active power $\Delta P_G$ to maintain the system's power balance, ultimately stabilizing the grid frequency at point $f_2$.

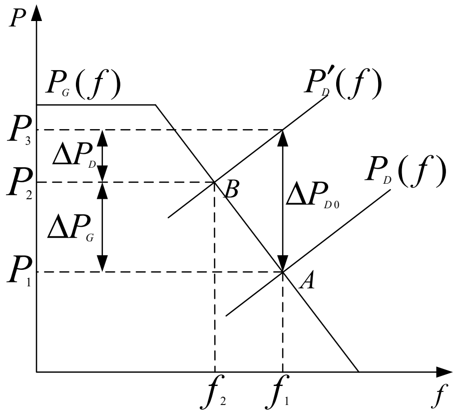


**Figure 4.** Primary frequency control.

### 3.2. Control Objectives of Primary Frequency Control

Figures 5 and 6 depict schematic diagrams illustrating the fast frequency response and active-frequency droop characteristics of wind farms and photovoltaic power stations, respectively. The renewable energy power generation system utilizes corresponding active control strategies and adds independent control devices to complete the active-frequency droop characteristic control, enabling it to have fast adjustment capabilities for participating in grid frequency regulation at the grid connection point. When the frequency at the grid connection point exceeds the frequency regulation dead zone, the frequency regulation control function is activated. Based on the active-frequency droop characteristic of the VSG, the active target value is calculated, and the control instructions are distributed to the DC/DC converter connected to the electrolytic hydrogen production device according to the active control strategy. Through the adjustment of the duty cycle, the voltage and current of the hydrogen production device are altered, thus changing the power consumption and efficiency of hydrogen production, and ensuring the grid frequency remains stable near the rated value.

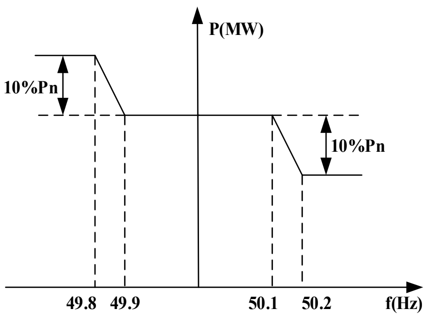


**Figure 5.** Fast frequency response and characteristics of wind farms.

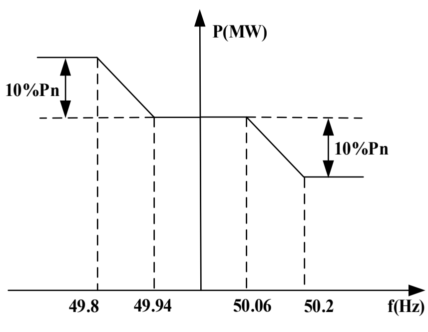


**Figure 6.** Fast frequency response and characteristics of photovoltaic power plants.

## 4. Strategy of Fast Frequency Response Control

### *4.1. System Structure*

The typical structure of a renewable energy power-generation hydrogen production system is illustrated in Figure 7. This system utilizes a hybrid AC/DC structure, as described herein, with wind turbines and photovoltaic modules functioning as power generation units that operate in MPPT mode by default. These units are connected to the DC bus via AC/DC and DC/DC converters. The electrolysis hydrogen production module serves as the energy storage unit, connected to the DC bus via a DC/DC converter and linked to the load and the grid via the grid-side converter. The grid-side converter employs VSG control to impart inertia and fast frequency response characteristics to the entire system, facilitating friendly grid connection. The electrolysis hydrogen production module serves as power support for VSG's primary frequency response, aiming to maintain the stability of the DC bus voltage.

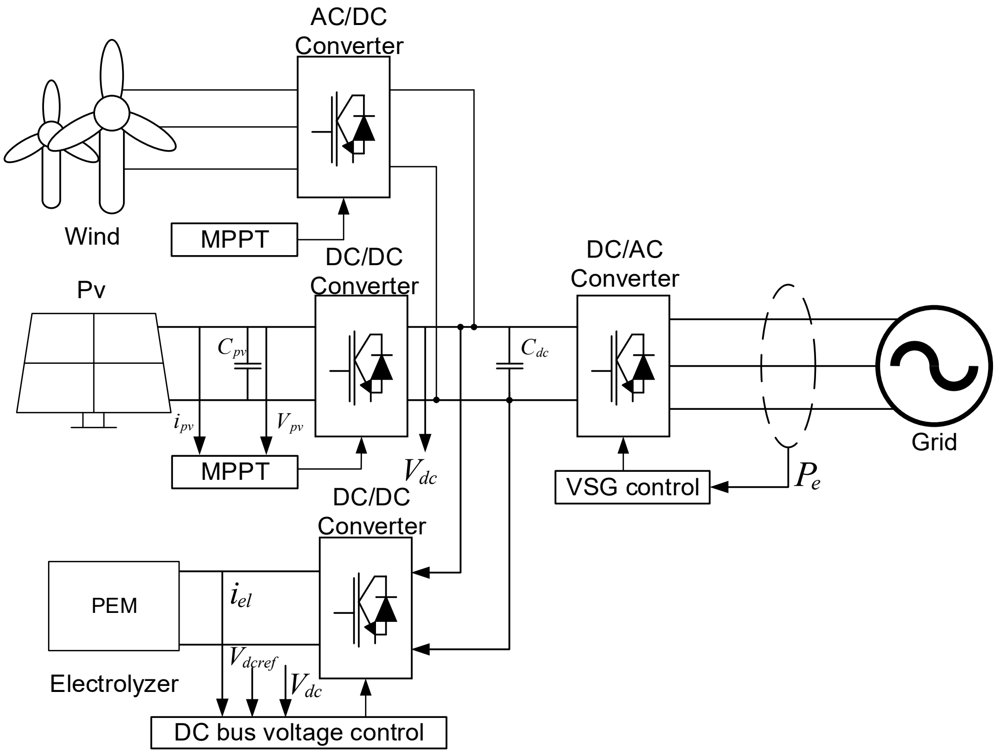


**Figure 7.** Renewable energy power-generation hydrogen production system.

### *4.2. DC/DC Converter Control Strategy on the Electrolyzer Side*

The excellent regulatory capabilities of the hydrogen production equipment by electrolysis provides favorable conditions for its participation in grid frequency regulation and improvement of the phenomenon of abandoned wind and solar energy generation systems. The electrolysis hydrogen production equipment is connected to the DC bus through a DC/DC converter. On the one hand, a stable power supply is essential for the smooth progress of the electrolysis process; on the other hand, the electrolysis hydrogen production equipment ensures system power balance via the converter, thereby maintaining DC bus voltage stability. Figure 8 illustrates the control strategy of the electrolysis hydrogen production equipment. The renewable energy generation system and VSG provide inertia and damping support for the grid. When the balance of DC side power and inverter output power changes, the DC bus voltage is disturbed. The electrolysis hydrogen production equipment promptly adjusts its own operating power to maintain a stable DC bus voltage, close to the reference voltage.

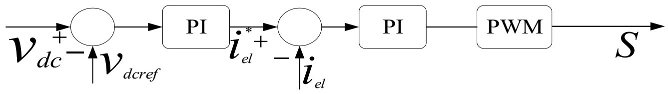


**Figure 8.** Control strategy for electrolyzer.

*4.3. DC/AC Converter Control Strategy on the Power Grid Side*

The grid-side converter adopts VSG control, which involves embedding the mathematical model of a synchronous generator into the control algorithm of the converter. This technology emulates a rotating motor by considering the static power electronic device to be a rotating machine. By emulating the primary frequency and voltage regulation of a synchronous generator, VSG equips the device with functions such as damping voltage and frequency fluctuations, automatic power allocation, and synchronous grid operation.

Figure 9 illustrates the structure and control block diagram of the virtual synchronous generator [18]. By embedding the synchronous generator equations in the converter control system, VSG can achieve power exchange between the DC power supply and the system according to the characteristics of the synchronous generator. When viewed from a system perspective and disregarding the high-frequency components caused by the switching action of power electronic devices, VSG is analogous to a synchronous generator. In a synchronous generator, both the mechanical shaft and winding are crucial in providing the necessary inertia and damping for the system's stable operation. For VSG, it is imperative to consider the establishment of virtual inertia and damping coefficients.

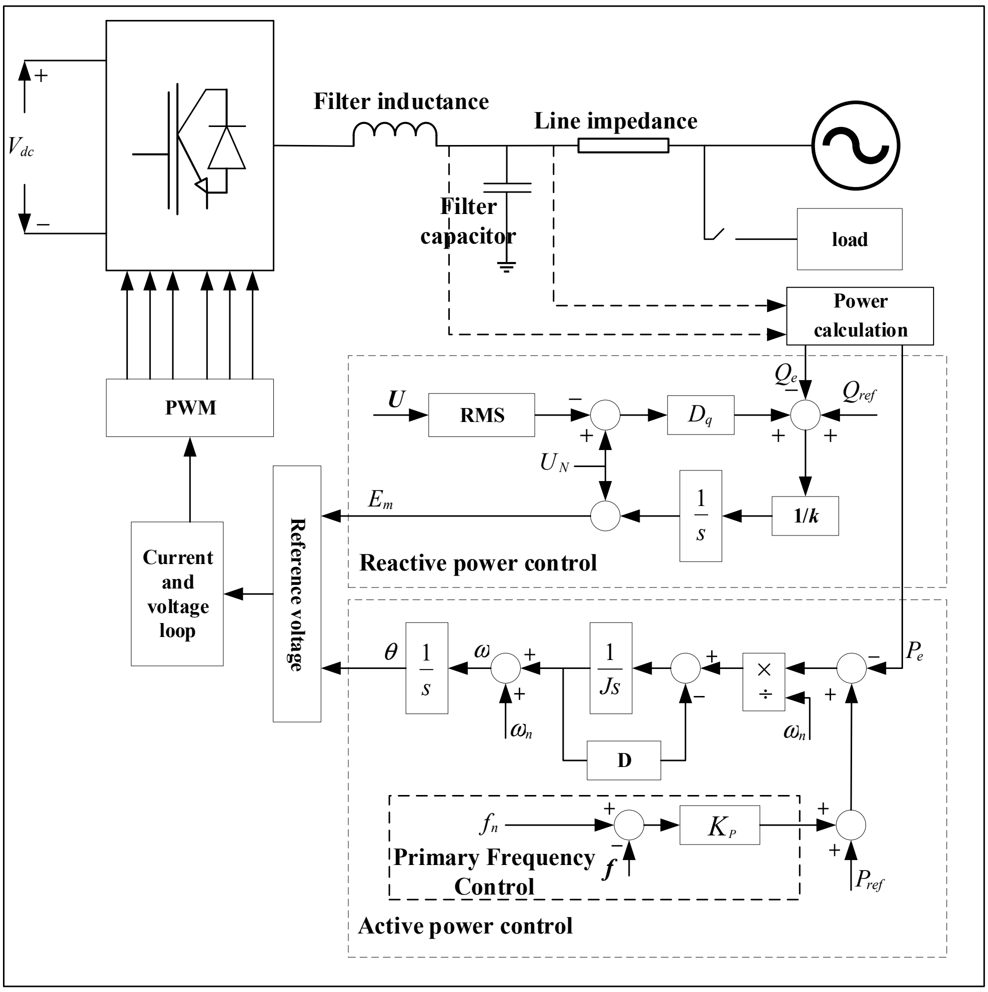


**Figure 9.** VSG structure and control block diagram.

The VSG rotor motion equation incorporates the second-order model of a traditional synchronous generator into the control mechanism, and Equation (11) demonstrates the inertial and damping characteristics of VSG [19].

$$\begin{cases} \omega = \frac{d\theta}{dt} \\ \frac{P_m - P_e}{\omega_n} - D(\omega - \omega_n) = J\frac{d\omega}{dt} \end{cases} \tag{11}$$

where $J$ is the virtual inertia coefficient, $D$ is the virtual damping coefficient, $\omega$ is the rotor angular velocity, $\omega_n$ is the rated rotor angular velocity, $P_m$ is the VSG theoretical output active power, and $P_e$ is the VSG actual output active power.

VSG emulates the $P$-$f$ droop characteristic of synchronous generators, thereby enabling the grid-side converter to achieve primary frequency control performance in grid-connected mode. Upon a disturbance in the grid frequency, the actual grid frequency calculated is compared with the reference value of the grid frequency, and the output power needed by the converter side is obtained according to the $P$-$f$ droop characteristic to regulate the frequency disturbance, thus fulfilling the primary frequency control function. The expression is as follows:

$$P_m = -K_p(f - f_n) + P_{ref} \tag{12}$$

where $P_{ref}$ is the active power reference value, $P_m$ is the VSG theoretical output active power, $K_p$ is the primary frequency modulation coefficient, $f$ is the grid actual frequency, and $f_n$ is the grid reference frequency.

## 5. Fast Frequency Response Control Parameters on Regulation Performance

### *5.1. The Impact of System Control Parameters on Regulation Performance*

Virtual rotational inertia and virtual damping coefficient constitute the core control parameters of the VSG control system. Therefore, based on the small-signal model of VSG active power, the transfer function is established as Equation (13) to study the influence of these two parameters on the system's dynamic characteristics [20].

$$G(s) = \frac{\frac{1}{J\omega_0}\frac{EU}{Z}}{s^2 + \left(\frac{D}{J} + \frac{K_\omega}{J\omega_0}\right)s + \frac{1}{J\omega_0}\frac{EU}{Z}} \tag{13}$$

The natural oscillation frequency $\omega_n$ and damping coefficient $\xi$ of the corresponding second-order model can be obtained according to Equation (13).

$$\begin{cases} \omega_n = \sqrt{\frac{EU}{J\omega_0 Z}} \\ \xi = D\sqrt{\frac{\omega_0 Z}{4JEU}} + K_\omega\sqrt{\frac{Z}{4J\omega_0 EU}} \end{cases} \tag{14}$$

Assuming the system is in an underdamped status, and selecting an error band $\Delta = 2\%$, the overshoot and adjustment time of the system are, respectively, as follows:

$$\sigma\% = e^{-\pi\xi/\sqrt{1-\xi^2}} \times 100\% \tag{15}$$

$$t_s = \frac{3.5}{\xi\omega_n} = 3.5/\left(\frac{D}{2J} + \frac{K_\omega}{2J\omega_0}\right) \tag{16}$$

Figure 10 illustrates the output power and frequency waveforms of the converter under different virtual inertia coefficients; Figure 11 illustrates the output active power and frequency waveforms of the converter under different damping coefficients. Upon analyzing the simulation diagrams in conjunction with Equations (15) and (16), it is observed that when the virtual damping coefficient is constant, an increase in the virtual rotational inertia results in greater output overshoot and a more pronounced oscillation; with the virtual rotational inertia remaining constant, a decrease in the virtual damping coefficient leads to greater overshoot, extended regulation time, and a more pronounced system oscillation.

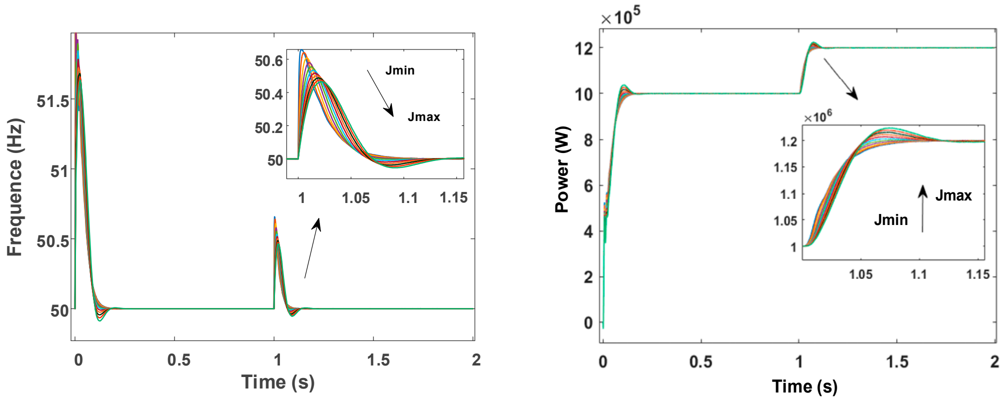


(**a**) (**b**)

**Figure 10.** Output power and frequency waveforms of converter under different virtual inertia coefficients. (**a**) Frequency. (**b**) Power.

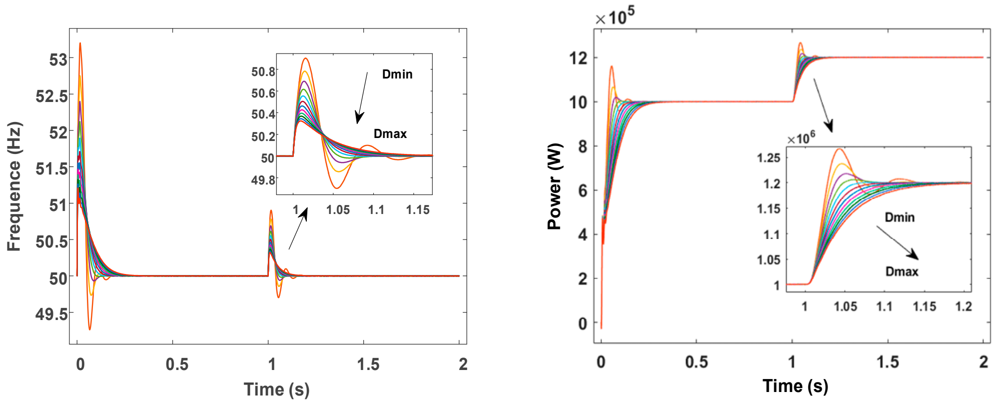


(**a**) (**b**)

**Figure 11.** Output power and frequency waveform converter under different damping coefficients. (**a**) Frequency. (**b**) Power.

### *5.2. Establishment of Control Parameter Optimization Model*

The core of VSG technology lies in the introduction of a simplified synchronous generator model into the converter control, enabling it to mimic synchronous generator characteristics. However, in comparison with actual synchronous generators, VSG is more flexible due to its ability to alter control parameters. Based on the analysis in the previous section, utilizing the particle swarm optimization algorithm to optimize the rotational inertia and damping coefficient of VSG facilitates more stable performance and faster response speed. The ITAE (Integral Time Absolute Error) index serves to establish the optimization objective function, as shown in Equation (17). The ITAE index may serve as a representative parameter for overshoot and regulation time, exhibiting minimal transient response oscillation.

$$ITAE = \int_0^t t \cdot |f - f_n| dt \tag{17}$$

where $t$ is the simulation time, $f$ is the grid actual frequency, and $f_n$ is the grid reference frequency.

### *5.3. Establishment of Adaptive Control Parameter Model*

When power fluctuations occur during the grid-connection process, the system frequency experiences decaying oscillations at the moment of fluctuations, and the overshoot and regulation time of the oscillations are key indicators for assessing the stability of the system frequency. The power angle characteristics and the angular velocity curve of synchronous generators are illustrated in Figures 12 and 13. The decaying oscillation process can be divided into four stages. The first stage system power increases from $P_1$ to $P_2$, resulting in a sudden increase in frequency. The angular velocity of the VSG is higher than the rated angular velocity of the grid, which is $\Delta\omega > 0$, and will continue to increase, $d\omega/dt > 0$. Therefore, it is necessary to increase the virtual inertia and damping coefficient to suppress $d\omega/dt$ and reduce the deviation of the angular frequency. In the second stage, system power increases from $P_2$ to $P$, during which $\Delta\omega > 0$, $d\omega/dt < 0$ need to reduce the virtual inertia to accelerate the adjustment of $\omega$, stabilizing its curve to the rated angular velocity, while appropriately reducing the damping coefficient. The third and fourth stages are similar to the first and second stages [21].

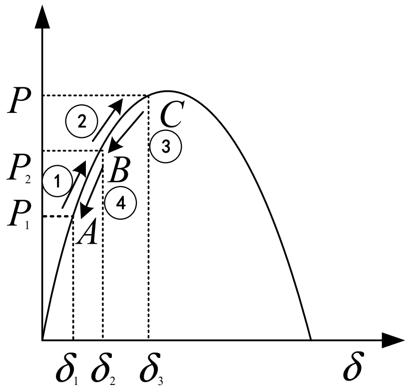


**Figure 12.** Synchronous generator power angle characteristic curve.

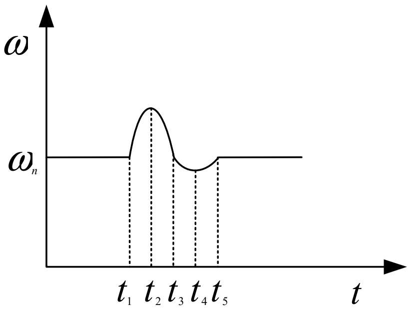


**Figure 13.** Synchronous generator angular velocity curve.

According to the above analysis, the selection principles of inertia and damping coefficients under different conditions are shown in Table 1. Combining the optimized initial inertia and damping coefficients based on the particle swarm optimization, an adaptive control strategy is designed as Equations (18) and (19).

$$J = \begin{cases} J_0 & \left|\frac{d\omega}{dt}\right| \le M_J \\ \max\left(J_0 + A\left|\frac{d\omega}{dt}\right| + B|\Delta\omega|, J_0 + J_1\right) & \Delta\omega \cdot \frac{d\omega}{dt} \ge 0 \cap \left|\frac{d\omega}{dt}\right| > M_J \\ \min\left(J_0 + C\left|\frac{d\omega}{dt}\right| + D|\Delta\omega|, J_0 - J_2\right) & \Delta\omega \cdot \frac{d\omega}{dt} < 0 \cap \left|\frac{d\omega}{dt}\right| > M_J \end{cases} \tag{18}$$

$$D = \begin{cases} D_0 & \left|\frac{d\omega}{dt}\right| \le M_J \\ \max\left(D_0 + E\left|\frac{d\omega}{dt}\right| + F|\Delta\omega|, D_0 + D_1\right) & \Delta\omega \cdot \frac{d\omega}{dt} \ge 0 \cap \left|\frac{d\omega}{dt}\right| > M_J \\ \min\left(D_0 + G\left|\frac{d\omega}{dt}\right| + H|\Delta\omega|, D_0 - D_2\right) & \Delta\omega \cdot \frac{d\omega}{dt} < 0 \cap \left|\frac{d\omega}{dt}\right| > M_J \end{cases} \tag{19}$$

where $J_0$ and $D_0$ represent the initial inertia coefficient and damping coefficient of the VSG after particle swarm optimization, $M_J$ is the $d\omega/dt$ transformation threshold, *A*-*D* and *E*-*H* are the adjustment coefficients for the moment of inertia and damping coefficient, and $J_1$, $J_2$, $D_1$, and $D_2$ are the support coefficients for the moment of inertia and damping coefficient.

**Table 1.** Principles for selecting $J$ and $D$ in different situations.

| Phase | Variation | Change Rate | $J$ | $D$ |
|---|---|---|---|---|
| A | $\Delta\omega > 0$ | $\frac{d\omega}{dt} > 0$ | Increase | Increase |
| B | $\Delta\omega > 0$ | $\frac{d\omega}{dt} < 0$ | Reduce | Reduce |
| C | $\Delta\omega < 0$ | $\frac{d\omega}{dt} < 0$ | Increase | Increase |
| D | $\Delta\omega < 0$ | $\frac{d\omega}{dt} > 0$ | Reduce | Reduce |

### *5.4. The Process of Parameter Optimization*

Through the introduction of an optimization model for control parameters and an adaptive control parameter model, we have established a method for optimizing the parameters of a combined particle swarm optimization and adaptive VSG control strategy. The specific optimization process proceeds as follows:

(a) Initialize particle parameters.
(b) Calculate the ITAE value based on the VSG output frequency.
(c) Update the individual best values and the global best solution based on the individual and overall ITAE values, finding the most suitable $J$ and $D$ for this iteration.
(d) Modify the $J$ and $D$ of the VSG based on the particle swarm's individual update formula.
(e) After 20 iterations, calculate the ITAE value to complete optimization, and display the optimized $J$ and $D$.
(f) Conduct a grid-connected simulation using the optimized $J_0$ and $D_0$.
(g) Monitor the VSG output angular frequency and angular frequency rate changes during operation.
(h) Determine if the VSG output angular frequency rate exceeds the threshold.
(i) If the threshold is exceeded, adaptively adjust the VSG's moment of inertia and damping coefficient online, based on the designed VSG control parameters.

## 6. Case Study

### *6.1. Case Description*

To verify the effectiveness of the control strategy of hydrogen production systems based on renewable energy power, a system simulation model was built on the Matlab/Simulink platform, as illustrated in the structure in Figure 7. In this system, the rated capacity of the photovoltaic power generation is 1.22 MW, the rated capacity of the wind power generation is 1.06 MW, the rated capacity of electrolytic hydrogen production equipment is 1.2 MW, and the DC bus voltage is 2500 V. The system connects to a public grid with a rated frequency of 50 Hz.

### *6.2. Simulation of Coordinated Control Strategy*

Based on the above system, two disturbance events were established to analyze the electrolytic hydrogen production device's ability to actively adjust the hydrogen production power when there is an excess of electricity in renewable energy. The specific process is as follows:

(1) When t = 1.5 s, the light intensity increased from 800 W/m$^2$ to 1000 W/m$^2$.
(2) When t = 3 s, the wind speed increased from 10 m/s to 12 m/s.

Figures 14 and 15 illustrate the results of the grid-connected simulation of the hydrogen production system based on renewable energy power. It can be seen that at t = 1.5 s, the illumination intensity increased from 800 W/m$^2$ to 1000 W/m$^2$, and the photovoltaic output power increased from 0.98 MW to 1.22 MW; at t = 3 s, the wind speed increased from 10 m/s to 12 m/s, and the wind turbine output power increased from 0.61 MW to 1.05 MW. The output power limit at the grid connection point is 1 MW. When there was excess electricity in renewable energy, the electrolysis hydrogen production power increased by 0.24 MW at t = 1.5 s and 0.39 MW at t = 3 s, respectively.

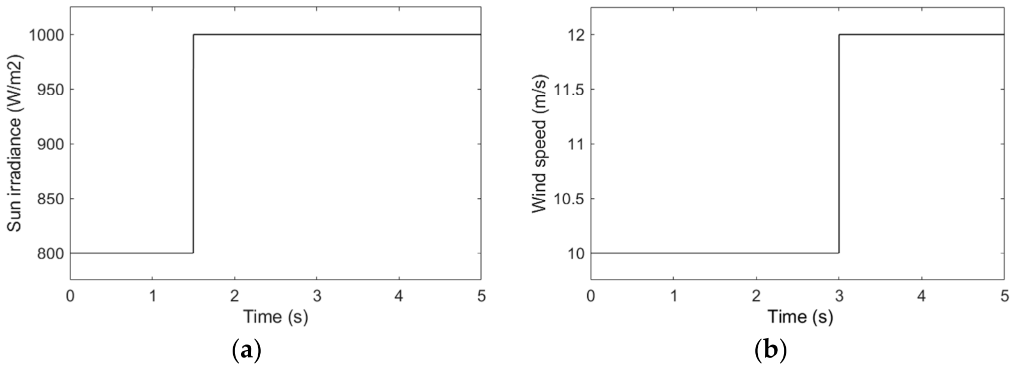


**Figure 14.** (**a**) Sun irradiance. (**b**) Wind speed.

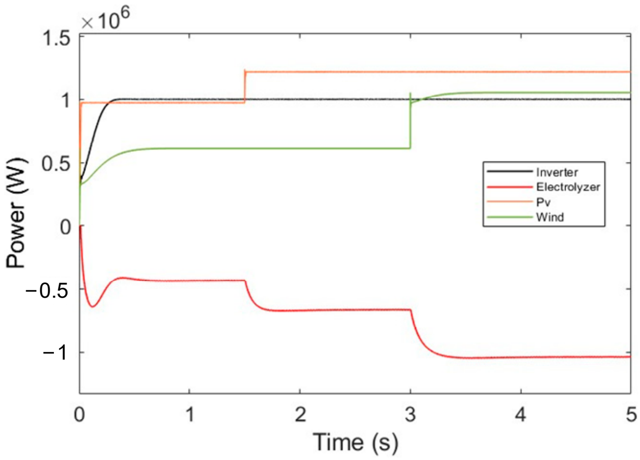


**Figure 15.** Wind, Pv, electrolyzer, and inverter output power.

### *6.3. Simulation of Fast Frequency Response Control Strategy*

Based on the above system settings, we analyzed the rapid frequency response capability of the grid connection interface of hydrogen production system based on renewable energy power generation. The specific process is as follows:

(1) When t = 1.5 s, disturbance in the external power grid leads to an increase in system frequency of 0.15 Hz;
(2) When t = 3 s, restore the system frequency to its rated value;
(3) When t = 4 s, the output power limit of the grid connection point has been increased from 1 MW to 1.2 MW.

Figures 16 and 17 illustrate the simulation results of the renewable energy power-generation hydrogen production system participating in the primary frequency control of the power grid. Figure 16a illustrates the output frequency of VSG, and Figure 16b presents the hydrogen production rate. Figure 17 presents the output power of wind turbines, photovoltaic cells, electrolyzers, and VSGs. It can be seen that the output power of photovoltaic cells and wind turbines remains constant at 1.22 MW and 0.61 MW, respectively. At t = 1.5 s, due to the disturbance of the external power grid, the system frequency increases by 0.15 Hz. VSG controls the DC/AC converter on the grid side according to its active power droop characteristic, reducing the output power from 1 MW to 0.855 MW. The electrolytic hydrogen production system quickly increases the hydrogen production power to 0.823 MW. At t = 3 s, the system frequency returns to the rated frequency of 50 Hz, and the output power of VSG also returns to 1 MW. The electrolytic hydrogen production system quickly reduces the hydrogen production power to 0.66 MW. At t = 4 s, the output power limit of the parallel point increases from 1 MW to 1.2 MW, resulting in a 0.142 Hz output frequency disturbance of VSG. However, under the action of adaptive VSG control parameters, the frequency quickly returns to the rated frequency of 50 Hz, avoiding a long frequency recovery event. The electrolytic hydrogen production device adjusts the hydrogen production power to 0.43 MW. Throughout the process, the electrolytic hydrogen production system actively responds to the frequency disturbance of the power system and participates in the primary frequency control of the power system. The hydrogen production rate also continuously varies with the electrolytic power.

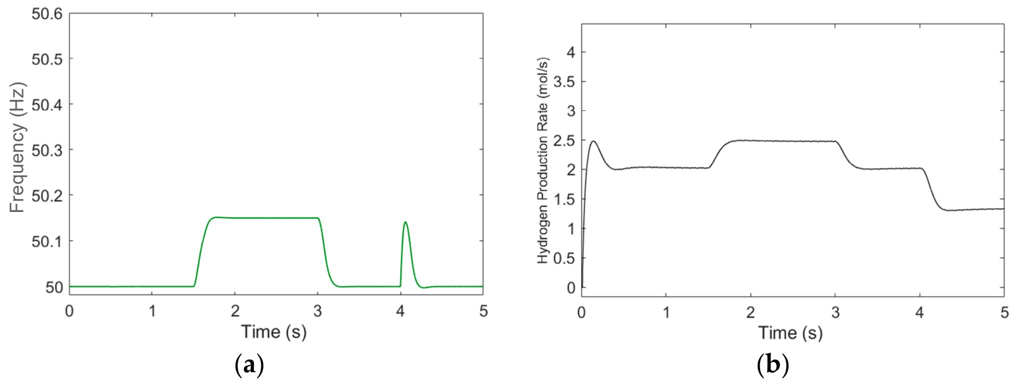


**Figure 16.** (**a**) VSG output frequency. (**b**) Hydrogen production rate.

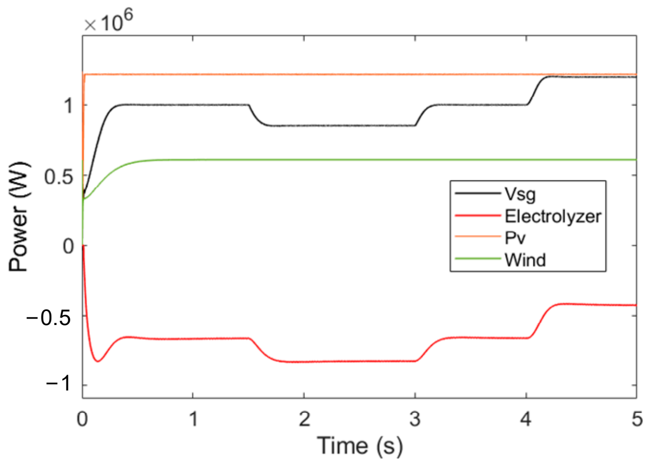


**Figure 17.** Wind, Pv, electrolyzer, and inverter output power.

Figure 18 illustrates the DC bus voltage waveform. It can be seen that at t = 0 s, t = 1.5 s, t = 3 s, and t = 4 s, the system experiences power imbalance and brief disturbances. However, due to the power support provided by the electrolytic hydrogen production system, the DC bus voltage remains close to the set value of 2500 V.

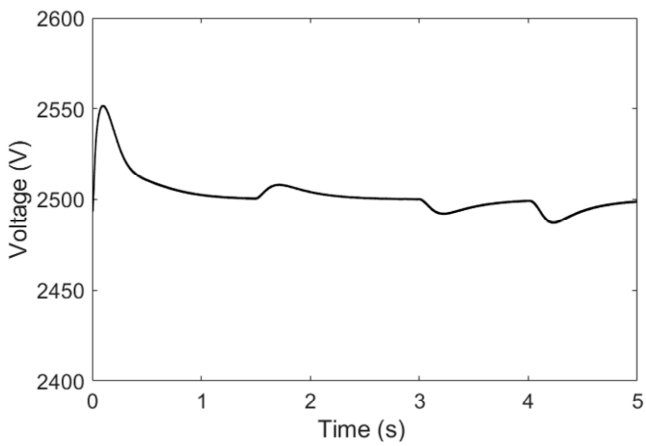


**Figure 18.** DC bus voltage.

### 6.4. Comparative Analysis of Parameter Optimization

To demonstrate the superiority of combining the particle swarm optimization algorithm with adaptive VSG control strategy, frequency and power curves obtained from simulations under identical working conditions for varying inertia and damping coefficients are illustrated in Figure 19. Mode 1 adopts the traditional VSG control strategy; Mode 2 employs the VSG adaptive control strategy without particle swarm optimization; Mode 3 initializes the rotational inertia and damping coefficients via the particle swarm optimization algorithm, without the use of an adaptive algorithm; Mode 4 combines the particle swarm optimization algorithm with adaptive control parameters.

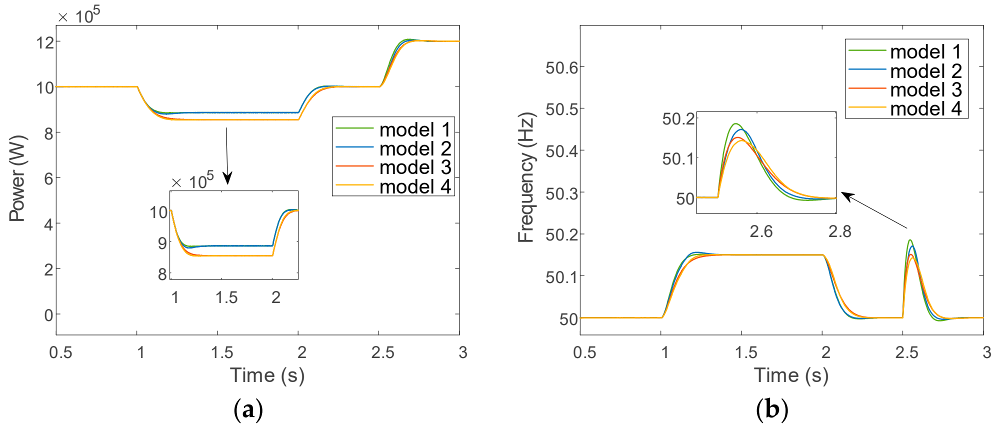


**Figure 19.** Frequency and power curve under different control parameter modes. (**a**) Frequency curve comparison chart. (**b**) Power curve comparison chart.

To study the advantages of the control strategy proposed herein, a comparison was conducted with traditional control strategies based on a fixed moment of inertia and damping coefficients. As illustrated in Figure 19a, at t = 2.5 s, a fluctuation in the VSG output power was observed. Under the traditional control strategy with fixed moment of inertia and damping coefficients, the overshoot of VSG output power was 1.6%, with a regulation time of 0.246 s. As illustrated in Figure 19b, the frequency fluctuation was 50.186 Hz. In contrast, under the adaptive control strategy proposed in this paper, the overshoot of VSG output power was reduced to 0.58%, with a regulation time of 0.187 s. Additionally, from Figure 19b, the frequency fluctuation was measured to be 50.143 Hz.

To highlight the importance of particle swarm optimization in determining the initial moment of inertia in this paper, a comparison was made with the VSG adaptive control strategy proposed in this paper alone. As illustrated in Figure 19, it can be observed that from t = 1 s to t = 2 s, the VSG participated in primary frequency regulation of the grid. Compared to the control strategy before optimization, the application of particle swarm algorithm to optimize the initial damping coefficient and moment of inertia resulted in an increase of 0.31 MW in the primary frequency regulation power, indicating a stronger primary frequency regulation capability.

At t = 2.5 s, fluctuations in VSG output power were observed. Under the VSG adaptive control strategy without particle swarm optimization, the overshoot of VSG output power was 0.88%, with a regulation time of 0.225 s, and a frequency fluctuation of 50.171 Hz. In the adaptive control strategy proposed in this paper that incorporates particle swarm optimization, the overshoot of VSG output power decreased by 0.3%, the regulation time reduced by 0.038 s, and the frequency fluctuation decreased by 0.028 Hz.

## 7. Conclusions

This article addressed the issue of the lack of autonomous frequency regulation capabilities in renewable energy power-generation systems. A structural model of coupling renewable energy power-generation systems with electrolytic hydrogen production systems to participate in rapid frequency response of a grid was established, and the dynamic regulation characteristics of the electrolysis hydrogen production system were verified through a Simulink simulation. When the power conversion of the renewable energy system and the grid frequency fluctuated, the electrolysis hydrogen production system was able to adjust its operating power accordingly, thus actively maintaining the system power balance and the stability of the DC bus voltage as well as participating in primary frequency control of the grid. Additionally, aiming at solving the problem of fixed inertia and damping coefficient in traditional VSG control strategies, a Simulink simulation was built to compare the influence of different control parameters on a system's active power and frequency. A VSG control strategy that combines particle swarm optimization and adaptive control parameters was proposed to enhance the primary frequency control capability of the entire system and improve the response characteristics of system frequency and output active power. This paper, by incorporating control strategies, transformed the electrolytic hydrogen production device from a simple power load into a flexible regulation resource in the power system, supporting grid frequency disturbances at the millisecond timescale. It also addressed the issue that renewable energy generation, serving as a power electronic interface, lacks the inertia, damping, and primary frequency control capabilities of traditional synchronous generators under disturbance conditions. However, current research only focuses on single-machine systems, and future studies will investigate the consistency of fast frequency response control for multiple renewable energy generation and hydrogen production systems, considering the uncertainty of communication environments.

**Author Contributions:** Conceptualization, T.S.; formal analysis, T.S.; writing—review and editing, T.S.; supervision, T.S.; project administration, T.S.; funding acquisition, T.S.; methodology, T.S., Z.X. and L.G.; software, Z.X.; data curation, Z.X.; writing—original draft preparation, Z.X.; visualization, Z.X.; validation, Z.X. and H.Z.; investigation, L.G. and H.Z. All authors have read and agreed to the published version of the manuscript.

**Funding:** This work is supported by the major project of National Natural Science Foundation of China: "Theory and method of coordinated operation optimization of multi energy supply and demand system containing hydrogen" (No. 62192753).

**Data Availability Statement:** Derived data supporting the findings of this study are available from the corresponding author on request.

**Conflicts of Interest:** The authors declare no conflicts of interest.

## References

1. Liu, D.; Zhao, N.; Li, P.; Liu, M.; Xu, X.; Shao, P.; Cao, X. Market-Oriented Consumption Model Based on the Joint Tracking of Renewable Energy Generation Curve of "Shared Energy Storage & Demand Side Resources". *Dianwang Jishu/Power Syst. Technol.* **2021**, *45*, 2791–2800. [CrossRef]
2. Sheng, W.; Wu, M.; Ji, Y.; Kou, L.; Pan, J.; Shi, H.; Niu, G.; Wang, Z. Key Techniques and Engineering Practice of Distributed Renewable Generation Clusters Integration. *Proc. CSEE* **2019**, *39*, 2175–2186. [CrossRef]
3. Cai, G.; Chong, C.; Kong, L.; Long, P.; Hao, Z. Modeling and Control of Grid-Connected System of Wind/PV/Electrolyzer and SC. *Power Syst. Technol.* **2016**, *40*, 2982–2990.
4. Albarghot, M.; Rolland, L. MATLAB/Simulink Modelling and Experimental Results of a PEM Electrolyzer Powered by a Solar Panel. In Proceedings of the 2016 IEEE Electrical Power and Energy Conference (EPEC), Ottawa, ON, Canada, 12–14 October 2016; IEEE: Piscataway, NJ, USA, 2016; pp. 1–6. [CrossRef]
5. Valenciaga, F.; Evangelista, C.A. Control Design for an Autonomous Wind Based Hydrogen Production System. *Int. J. Hydrogen Energy* **2010**, *35*, 5799–5807. [CrossRef]
6. Sun, D.; Zheng, W.; Yu, J.; Li, J. Research on the Primary Frequency Regulation Control Strategy of a Wind Storage Hydrogen-Generating Power Station. *Electronics* **2022**, *11*, 3669. [CrossRef]
7. Agredano-Torres, M.; Xu, Q.; Zhang, M.; Söder, L.; Cornell, A. Dynamic Power Allocation Control for Frequency Regulation Using Hybrid Electrolyzer Systems. In Proceedings of the Conference Proceedings—IEEE Applied Power Electronics Conference and Exposition—APEC, Orlando, FL, USA, 19–23 March 2023; Institute of Electrical and Electronics Engineers Inc.: Piscataway, NJ, USA, 2023; Volume 2023, pp. 2991–2998. [CrossRef]
8. Veerakumar, N.; Ahmad, Z.; Adabi, M.E.; Torres, J.R.; Palensky, P.; van der Meijden, M.; Gonzalez-Longatt, F. Fast Active Power-Frequency Support Methods by Large Scale Electrolyzers for Multi-Energy Systems. In Proceedings of the 2020 IEEE PES Innovative Smart Grid Technologies Europe (ISGT-Europe), The Hague, The Netherlands, 26–28 October 2020; IEEE: Piscataway, NJ, USA, 2020; pp. 151–155. [CrossRef]

9. Sarrias-Mena, R.; Fernández-Ramírez, L.M.; García-Vázquez, C.A.; Jurado, F. Electrolyzer Models for Hydrogen Production from Wind Energy Systems. *Int. J. Hydrogen Energy* **2015**, *40*, 2927–2938. [CrossRef]
10. Zhang, X.; Gao, Q.; Guo, Z.; Zhang, H.; Li, M.; Li, F. Coordinated Control Strategy for a PV-Storage Grid-Connected System Based on a Virtual Synchronous Generator. *Glob. Energy Interconnect.* **2020**, *3*, 51–59. [CrossRef]
11. Zhong, Q. Virtual Synchronous Machines and Autonomous Power Systems. *Proc. CSEE* **2017**, *37*, 336–348. [CrossRef]
12. Cheng, Q.; Yu, D.; Cheng, Y.; Gao, J.; Zhang, Y.; Tan, F. Control Strategy of Virtual Synchronous Generator Based on Adaptive Rotational Inertia. *Electr. Power Autom. Equip.* **2018**, *38*, 79–85. [CrossRef]
13. Gao, F.; Qian, K.; Li, M.; Jiang, Y.; Li, T.; Wen, B. Control Strategy of Virtual Synchronous Generator Based on Self-Adaptive Damping Control Algorithm. *Power Capacit. React. Power Compens.* **2021**, *42*, 109–114. [CrossRef]
14. Yang, Y.; Mei, F.; Zhang, C.; Liao, H.; Chen, H.; Zheng, J. Collaborative Adaptive Control Strategy for Virtual Synchronous Generator's Rotational Inertia and Damping Coefficient. *Electr. Power Autom. Equip.* **2019**, *39*, 125–131. [CrossRef]
15. Falcão, D.S.; Pinto, A.M.F.R. A Review on PEM Electrolyzer Modelling: Guidelines for Beginners. *J. Clean. Prod.* **2020**, *261*, 121184. [CrossRef]
16. Ma, Z.; Witteman, L.; Wrubel, J.A.; Bender, G. A Comprehensive Modeling Method for Proton Exchange Membrane Electrolyzer Development. *Int. J. Hydrogen Energy* **2021**, *46*, 17627–17643. [CrossRef]
17. Görgün, H. Dynamic Modelling of a Proton Exchange Membrane (PEM) Electrolyzer. *Int. J. Hydrogen Energy* **2006**, *31*, 29–38. [CrossRef]
18. Ling, Z.; Liu, Y.; Wang, Z.; Yin, J. Adaptive Inertia and Damping of Grid-Connected Inverter with Improved VSG Control. *IET Power Electron.* **2023**, *16*, 2769–2781. [CrossRef]
19. Ding, L.; Ke, S.; Yang, J.; Shi, X. Control Strategy of Virtual Synchronous Generator Based on Adaptive Control Parameter Setting. *Integr. Intell. Energy* **2023**. Available online: https://kns.cnki.net/kcms/detail/41.1461.TK.20230823.0909.002.html (accessed on 27 February 2024).
20. Shen, Z.; Liu, Y.; Zheng, B.; Qi, Y.; Li, J. Microgrid Optical Storage Charge and Discharge Control Technology Based on Adaptive Virtual Synchronous Generator. *Distrib. Energy* **2021**, *6*, 18–25. [CrossRef]
21. Zheng, T.; Chen, L.; Wang, R.; Li, C.; Mei, S. Adaptive Damping Control Strategy of Virtual Synchronous Generator for Frequency Oscillation Suppression. In Proceedings of the 12th IET International Conference on AC and DC Power Transmission (ACDC 2016), Beijing, China, 28–29 May 2016; Institution of Engineering and Technology: Stevenage, UK, 2016; pp. 1–5. [CrossRef]